SATELLITE CONJUNCTIONS IN THE RF SPECTRUM: RESULTS FROM AN RF MEASUREMENT CAMPAIGN OF LEO OBJECTS

Valentin Eder, Philip Letfus, and Christian Unfried

Space Analyses GmbH, Marxergasse 24/2, A-1030 Wien, Austria,
e-mail: {valentin.eder,philip.letfus,christian.unfried}@spaceanalyses.at

ABSTRACT

The Radio Frequencies (RF) Spectrum is, on the one hand an important factor of successful satellite operations and satellite-based services, but on the other hand a limited natural resource. The increased commercial activities, especially in lower earth orbits, have a direct impact on the availability of satellite services, the safety of operations and the 'dark and quiet skies' topics.

Classical carrier monitoring systems from established providers were developed mainly to monitor GEO objects. They are working in a round-robin cycle to record RF measurements, also mainly applying highly sufficient signal intelligence. However, this approach lacks systematic measurements in correlation with LEO objects.

To overcome this hurdle, Space Analyses has developed a new three-dimensional object measurement system (THRIMOS) with the help of ESA funding in the ARTES program line. This new system was used to perform a measurement campaign in October and November 2024 to seek answers to the question if any evidence of interference can be found between two large satellite constellations in the downlink payload traffic and if that is the case, how big the impact on the satellite service availability would be.

Until end of November 2024, more than 7200 measurements were taken. These measurements were able to confirm the interference between the two satellite constellations. Based on the counts of recorded interference events, it was possible to estimate availability figures.

The results showed a significant impact in the service availability of at least one constellation. The resulting figures of the estimated user service availability were dropping below 99.5%.

Keywords: Radio Frequency; RF Conjunction; Satellites; Constellations; RF Spectrum; Interference.

1. INTRODUCTION

The radio frequency (RF) spectrum is a critical component for multiple space-based services, including telecommunication, astronomy, weather forecasting and others [12]. However, the increasing commercialization of the low Earth orbit (LEO) has led to a significant increase in the number of active and passive space objects [5] and therefore to the question of detectable interference between different satellite constellations in downlink payload traffic and, if this interference can be found, the potential implications [10] for the availability of the said satellite services.

Until now, due to the lack of empirical data, the urgency of this problem was difficult to assess. Therefore, systematic measurements were needed to make a well-founded statement about the presence and impact of interference. To address this question, the goal was to collect empirical evidence of possible interference between two large satellite constellations and to quantify their impact on service availability.

2. SPECTRUM MONITORING GROUND STATIONS

Satellite tracking and spectrum monitoring is carried out via ground stations, which use receiving systems, often coupled to a spectrum analyser, a device used to measure the strength of an RF signal over a defined band of frequencies of received (RX) and transmitted (TX) signals radio frequency. Fig. 1 illustrates the key parameters involved in this process..

2.1. Ground Station Antenna Pointing

The Ground Station antenna pointing describes the horizontal and vertical angle between the horizontal plane of the ground station and the current pointing of the antenna into the sky. An elevation near 90° means the satellite is almost directly above the station, while a low elevation

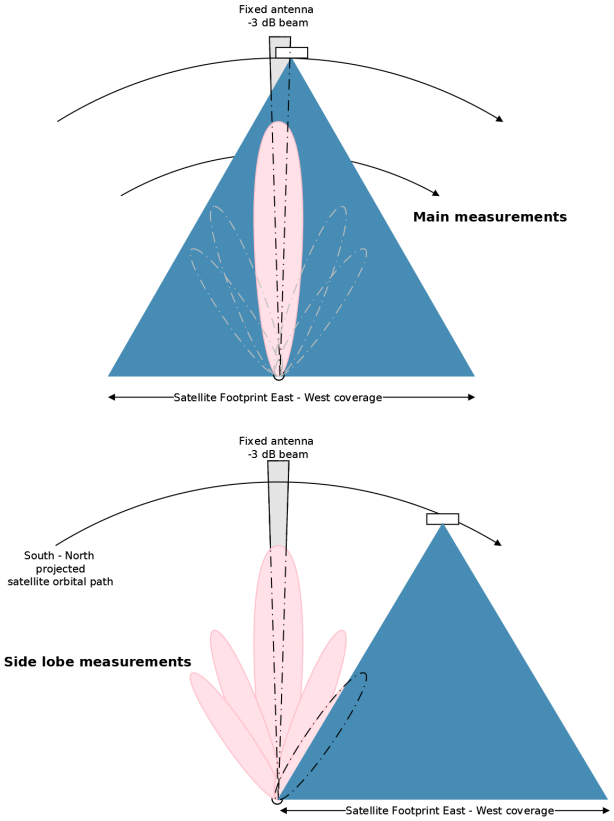

Figure 1. A satellite approaches a ground station. The blue cone is the satellite down link beam and the grey cone is the satellite antenna beam. Due to the wide down link beam the signal of the satellite might already covering the Rx antenna but no signal is recorded. Never the less there might be signal recordings via antenna side lobes.

indicates the satellite is close to the horizon [4]. A display of this can be seen in Fig. 2.

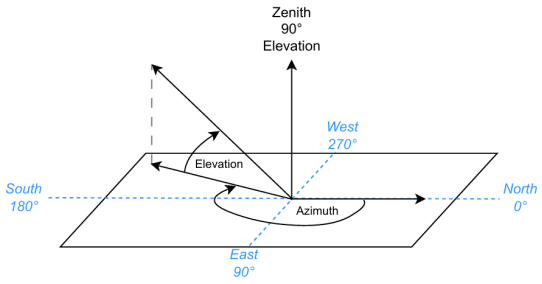

Figure 2. Ground station antenna pointing

2.2. Slant Path

The Slant Path refers to the effective path the signal travels between the ground station and the satellite. [3].

2.3. Crossing Path Length

The Crossing Path Length describes the time and distance a satellite spends in the field of view of a ground station. This length is determined by the the satellite's orbit, the object's speed, and the observation geometry of the ground station.

2.4. TX and RX Frequencies

Ground stations communicate with satellites via defined frequency bands. The choice of TX (transmission) and RX (reception) frequencies depends on several factors, including the satellite's operating mode.

2.5. Half width / -3 dB angle

The half-width (HW) angle is a more general term that describes the angular range in which a measured value drops to half its maximum value. In antenna patterns, the -3 dB angle determines the width of an antenna's main radiation pattern and thus how precisely a ground station or satellite must be aligned.

3. EXPECTED LIMITATIONS

3.1. Geometric accuracy definitions

The orbital path of objects in near-earth space can be defined in the following directions (See Fig.3):

- Radial (U): The direction of the position vector
- Cross-track (W) : Direction of the angular momentum
- In-Track (V) : $W \times U$

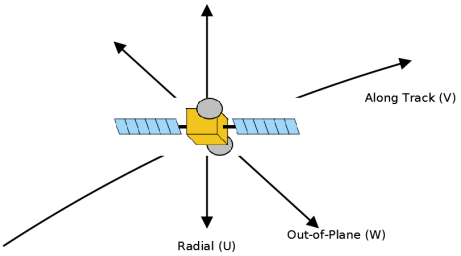

Figure 3. Accuracy direction definitions

Assuming a spacecraft RF transmitting beam points toward the Earth's centre, the radial position (U) has minimal influence on RF emissions' monitoring ground station recording usability. Measurement accuracy is influenced by:

- Antenna opening angle (Antenna size and frequency) with Orbital height of the RF object at the line of (measurement) sight
- Antenna pointing error
- Timing information
- Orbital position information
- Orbital path prediction algorithm and RF conjunction calculation algorithm

A schematic representation of a possible ideal pointed opening angle of a -3 dB antenna cone around a satellite can be seen in Fig. 4.

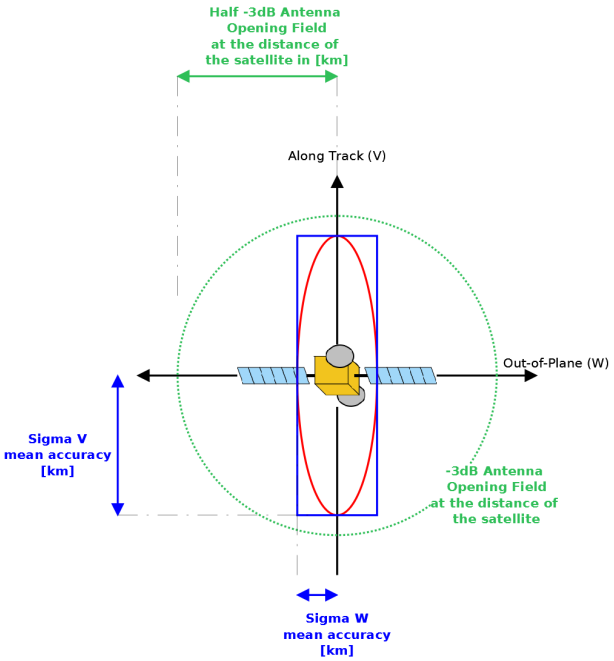

Figure 4. The green circle represents the opening field of the antenna at the distance of the satellite. Sigma indicates the mean accuracy of the measurement.

An illustration of an object flying through an antenna beam (drawn from the side in the direction of cross track) with the possible accuracy errors can be seen in Fig. 5.

Antenna opening angle (Antenna size and frequency) and Orbital height of the RF object at the line of (measurement) sight

Contrary to the display in Fig. 4, the elevation of the antenna might not be always 90°, which also means that the orbital height is les than the complete slant path. The length of the path within the -3 dB antenna cone is a function of frequency, antenna diameter, orbital height of the object, and antenna elevation angle.

The antenna cone opening path L (Eq. 1,see also Fig. 5)

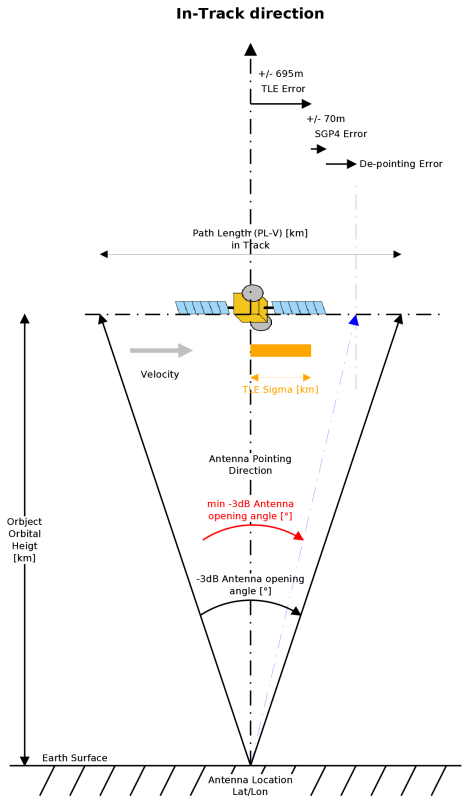

Figure 5. This diagram illustrates an object flying from one side through an antenna beam defined by its -3 dB opening angle.

can be calculated using trivial trigonometric identities.

$$L = \frac{2 \cdot h}{cot(\varepsilon)} \tag{1}$$

In Eq. 1, h is the altitude of the Satellite and ε is the opening angle. Note that the opening angle depends on the frequency of the satellite signal. An example of this relation can be seen in Fig. 6.

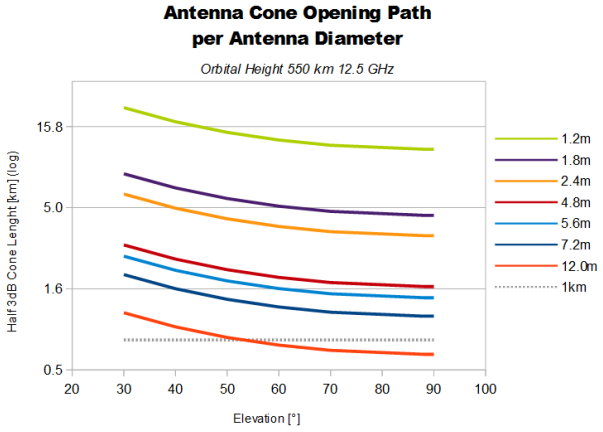

Figure 6. Antenna Cone Opening Path at 12.5 GHz for different antenna diameters

Antenna pointing error

The antenna pointing accuracy can be defined by

- Relative Pointing Error (RPE): the angular separation between the instantaneous absolute orientation of the satellite fixed axis at a given time and a reference axis defined over 30 s around that time. This is a measure of the jitter of the satellite and is expressed as 2σ, half-cone;
- Absolute Pointing Drift (APD): the angular separation between the short time average (barycentre of the actual pointing during a given time interval) and a similar pointing at a later time;
- Absolute Pointing Error (APE): the angular separation between the commanded direction and the actual direction, effectively blind pointing accuracy. It is defined as in Eq. 2 [13]

$$APE = 2 \cdot \sqrt{\sigma_y^2 + \sigma_x^2} \tag{2}$$

A typical reference for the accuracy of the pointing-error given from Sea Tel for antennas < 2.4 m is better than $0.2°$ [7]. A typical reference for the pointing accuracy given by Safran for antennas > 2.4 m is ≤ 40 m° rms [14].

A typical reference for a pointing accuracy is given by Calian for a 4 m antenna with < 0.018 [1].

As the pointing accuracy is also given in degree in analogy to the -3 dB antenna opening angle, the de-pointing accuracy contributes to the error in the amount of about 4% of the antenna opening angle and correlates linearly with the antenna opening path.

Timing information

Time plays a central role in the plan to measure objects flying through a fixed antenna beam. Time is involved in

- Time synchronisation of the measurement system elements
- Time from the orbital predictions
- Time to start and stop the measurement device (control loop)
- Variations in the speed of objects due to orbital manoeuvres, resulting in different arrival times in the antenna beam

Orbital position information

Estimates of the accuracy of TLEs can be found in the public available literature [6].

Orbital path prediction algorithm

The error contribution of the SGP4 orbital prediction, which is used for TLEs, is $< 10\%$ of the accuracy of the TLE information [2].

3.2. Satellite pointing direction

Satellite pointing influences the timing and signal strength of recorded measurements. Pitch, roll, and yaw variations can cause early, late, weak signal or even no-signal recordings (see Fig.7).

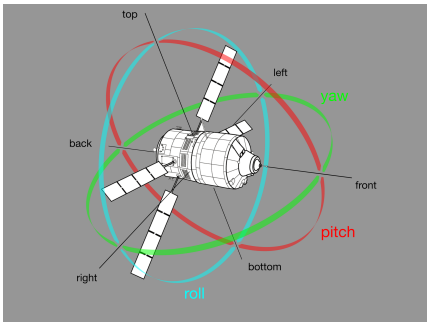

Figure 7. Satellite orientation directions [9]

The implementation of enabling RF measurements by setting time and RF parameters of events or scenarios where and when objects fly through various fixed ground stations led to the creation of the THRIMOS product.

4. METHODS

4.1. THRIMOS

The THRIMOS software uses Two Line Elements (TLEs) out of OMM data [8] and the SGP4 [15] propagation to estimate whenever a satellite is within the antenna beam of a ground station. As soon as an object is, according to the prediction, in the antenna beam of the selected ground station, THRIMOS triggers an RF measurement in the said ground station. These measurements are viewed in the "Result Explorer" tab of the software. Depending on the scenario of interest defined in the builder, THRIMOS also creates lists of whenever two satellites are passing within the same ground station antenna beam at the same time (so-called **RF conjunctions**).

To enable a systematic measurement environment, THRIMOS correlates measurements with space objects and builds so an RF catalogue of space objects containing recorded TX RF properties per object.

A catalogue entry shows the result of a measurement with the information of the space objects in the cone, the in-

formation of the ground infrastructure, the scenario of interest, portrays the trajectories in a graph (see Fig. 8) and the list of detected carriers of the measurement.

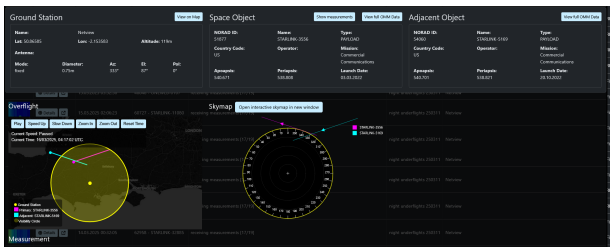

Figure 8. A measurement of a ground station in the Result Explorer in the THRIMOS SW

The software also shows a spectrum plot of the RF measurements, as well as the frequencies minimum, average and maximum (see Fig. 9), which will be used to find possible interferences.

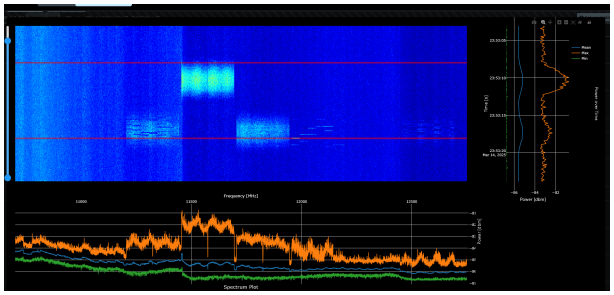

Figure 9. Details of the measurement of a ground station in the Result Explorer in the THRIMOS SW

Finally, THRIMOS also provides a detailed description of the detected frequencies (Fig. 10).

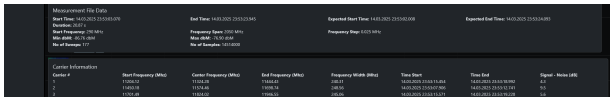

Figure 10. Carrier detection in THRIMOS

For the present study, RF conjunctions of a single ground station have been observed over a period of time. RF antenna beam crossings and RF conjunctions have been predicted. Out of RF conjunctions, the Interferences have been identified visually, the duration of the interference were determined from the axis of the graph that shows the frequency power, where the limit of the accuracy is the resolution of the time-axis. An example for this visual indicator can be seen in Fig. 11, where the orange frequency is the one of a OneWeb and the turquoise frequency the one of a Starlink satellite. The overlap indicates interference.

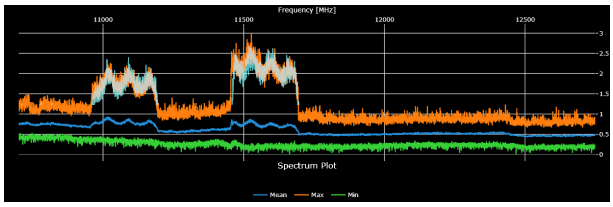

Figure 11. Visual interference: The orange and turquoise frequencies are from different satellites and they overlap.

4.2. Analysis of the data

Based on the frequency of the found interference events in the given duration of the measurements, we estimate the average time between two interferences (Eq. 3).

$$t_{interval}\ [\text{min}] = \frac{N_{days}}{N_{interferences}} \cdot 24 \cdot 60 \qquad (3)$$

After considering the monitoring area factor A_f, which is defined in Eq. 4 as the ratio of the monitoring areas of the ground stations opening angle and the -3 dB opening angle (since the interfering satellites orbit earth at different altitudes and thus have a different antenna pointing angle, see Fig. 1).

$$A_f = \frac{A_{\varepsilon_{open}}}{A_{\varepsilon_{HW}}} = \frac{r^2_{\varepsilon_{open}}\pi}{r^2_{\varepsilon_{HW}}\pi} = \left(\frac{\frac{d}{cot(\varepsilon_{open})}}{\frac{d}{cot(\varepsilon_{HW})}}\right)^2 \qquad (4)$$

we can get the number of interferences per day relative to area difference in Eq. 5

$$N = \frac{24 \cdot 60}{\frac{t_{interval}}{A_f}} = 1440 \cdot \frac{A_f}{t_{interval}} \qquad (5)$$

This can then be combined with the estimation of the duration of each interference and in conclusion be used to determine the availability of a ground station.

5. RESULTS

The measurement campaign ran from October 2024 to March 2025, recording over 50000 measurements. Among these, more than 3000 RF conjunctions involving more than one object in the antenna beam were identified. 6954 objects were catalogued, whereof 4410 had detectable carrier emissions. The system identifies on average 2,200 beam paths per week, where 85% results to real returned measurements.

A subset analysis from October to mid-November 2024 confirmed measurable interferences and identified five of these RF between OneWeb and Starlink satellites. The events were predicted with a SW and HW system developed and operated by Space Analyses GmbH Vienna. The Aaronia spectrum analyser V6 Plus 250XA [11] was

Figure 12. Antenna installation in UK for measurement recording

used as signal recording device. The recorded interference situations are listed in Tab. 1. These events, recorded from a fixed earth station in the UK (see Fig.12), confirmed measurable interference.

Additionally, in the course of the preparation of this paper, a second round of analytics was done in March 2025 and the authors identified four more interferences. For completeness, these findings are listed, but will not be further discussed.

Table 1. Interference events

Date	Time	Object	Duration [s] ($\pm$ 0.5)	Figure
02/10/24	19:49:35	ONEWEB 0595	4	13
17/10/24	08:02:16	ONEWEB 0082	5	14
01/11/24	10:21:00	ONEWEB 0651	3	15
10/11/24	08:40:40	ONEWEB 0595	4	16
10/11/24	19:38:53	ONEWEB-0676	5	17

In order to obtain the availability, we need to get the frequency of interferences $t_{interval}$ (Eq. 3 and Eq. 6) and compare it to the total time.

$$t_{interval}\ [\text{min}] = \frac{41}{5} \cdot 1440 = 11808\ \text{min} \tag{6}$$

The ground station monitoring area factor A_f from Eq. 4 for the ground station used is given through Eq. 7

$$A_f = \frac{2037037.94\ \text{km}^2}{1801.80\ \text{km}^2} = 1130.55 \tag{7}$$

The opening angle of the ground station used is $70°$ and the -3 dB opening angle is $2 \cdot 1.193°$.

Now, the number of interferences per day relative to the correction factor is given by Eq. 8.

$$N = 1440 \cdot \frac{1130.55}{(\frac{41}{5} \cdot 1440)} = 137.87 \tag{8}$$

For simplicity, we assume that each of the 5 interferences in 41 days lasted 4 seconds (this is roughly the average).

That means that the total duration of unavailability per ground station in a day is $137.87 \cdot 4$ s $= 551.48$ s $= 9.19$ min. This results in 99.36% availability per day.

In Tab. 3 in the appendix the dependency of the availability on the antenna opening angle (horizon elevation in °) and the interference duration in [s] in the case of 5 recorded interferences in 41 days with a 0.75 m standard parabolic antenna is shown.

5.1. Interference events, October 2024

In this section, the detected interference events will be displayed.

In Fig. 13, one can see an interference of one OneWeb satellite happening on the 02.10.2024 with one Starlink satellite sending at the same time, although very weakly present in the plot. In Fig. 14, one can see the display of

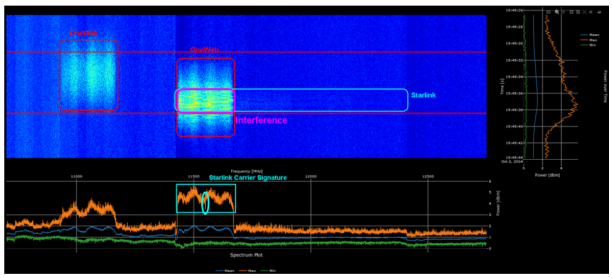

Figure 13. OneWeb-Starlink Interference 02.10.2024

an interference between a OneWeb and a Starlink satellite. They not only send at approximately the same time window, their signal has also a similar power level.

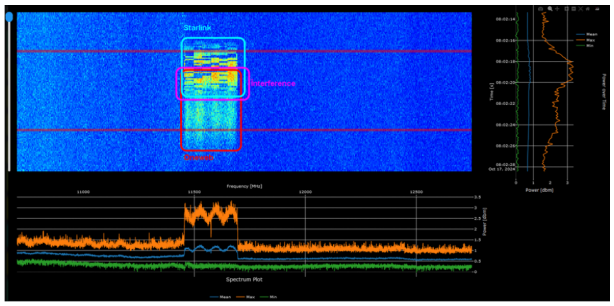

Figure 14. OneWeb-Starlink Interference 17.10.2024

Very similar effects can be seen in Fig. 15.

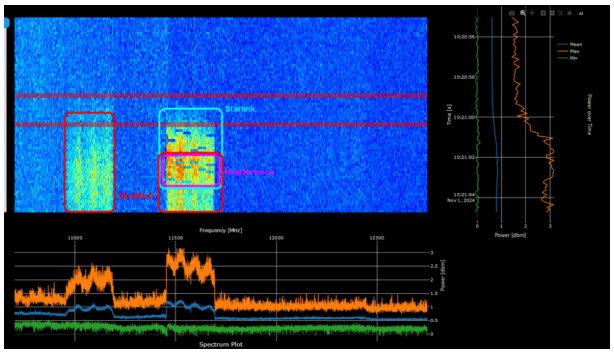

Figure 15. OneWeb-Starlink Interference 01.11.2024

Finally, on the 10.11.2024, another interference was measured as shown in Fig. 16.

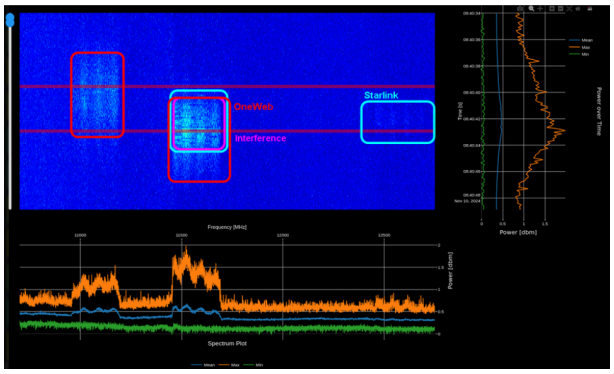

Figure 16. OneWeb-Starlink interference 10.11.2024

Last but not least an interference on the 14.11.2024 is shown in Fig. 17.

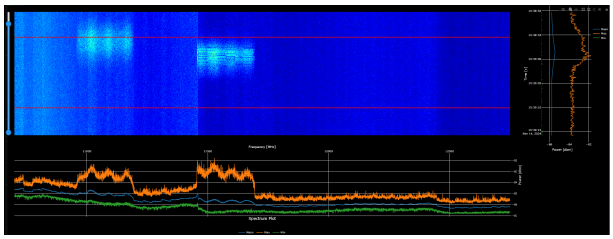

Figure 17. OneWeb-Starlink interference 14.11.2024

5.2. Interference events, March 2025

Four more interferences between the 13.3.25 and 19.3.25 are listed in Tab. 2 and can be seen from Fig. 18 to 21.

Table 2. Interference events in March 2025

Date	Time	Object	Duration [s] ($\pm$ 0.5)	Figure
13/03/25	21:54:30	ONEWEB 0277	4	18
15/03/25	05:54:53	ONEWEB 0141	4	19
15/03/25	23:46:47	ONEWEB 0277	5	20
17/03/25	14:01:49	ONEWEB 0202	4	21

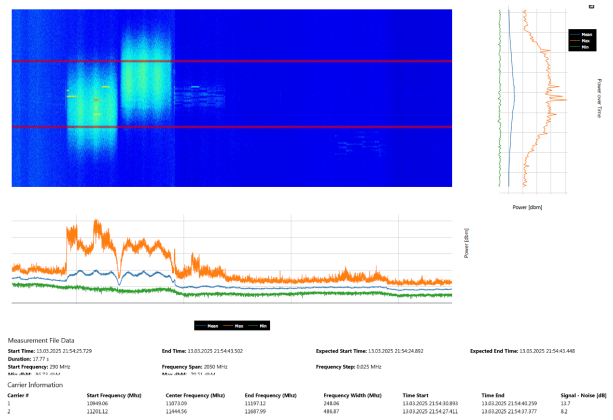

Figure 18. OneWeb-Starlink interference 13.03.2025 21:54:30

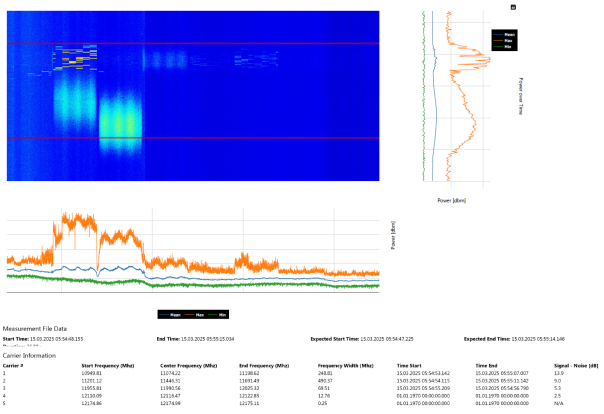

Figure 19. OneWeb-Starlink interference 15.03.2025 05:54:53

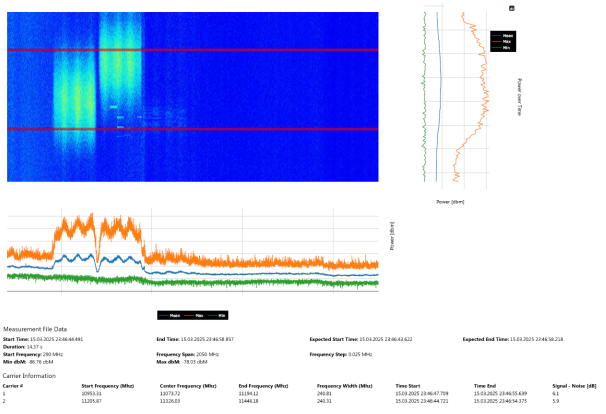

Figure 20. OneWeb-Starlink interference 15.03.2025 23:46:47

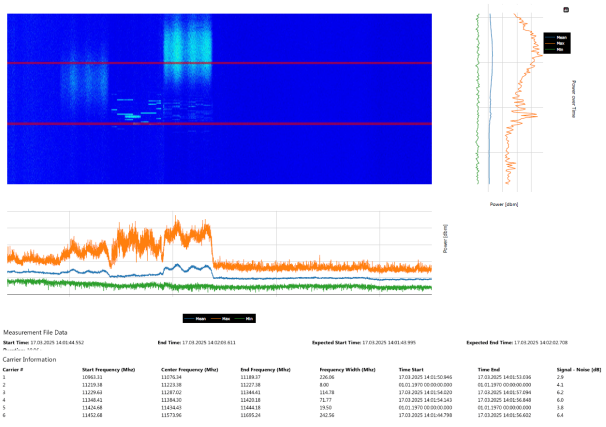

Figure 21. OneWeb-Starlink interference 17.03.2025 14:01:49

6. OUTLOOK

The increase in number of actively operated satellites, especially of those in commercial telecommunication fleets, but not only there, will increase the amount of RF conjunctions and interferences. In the interest of all stakeholders, evidence-based monitoring of the RF situation is indispensable to enable administrative and technical management of the RF resource. The given result raises questions of the implementation of frequency licences and regulations, technical mitigation possibilities, and, moreover, in the transparency of frequency use. The measurement campaign covered a frequency range of 2050MHz at the centre frequency of 11.725GHz which is undoubtedly most used in Ku customer traffic in the selected location of the ground station at 50.5° LAT what represents a hotspot of RF conjunction areas between OneWeb and Starlink. The open areas for future measurement campaigns (and the necessary 24/7 monitoring) are the frequencies from the S band up to the extended Ka band (including all X bands) with a focus on frequencies used by TT&C, and the spatial extension to other latitude areas (equatorial regions). To technically enable efficient and systematic monitoring, the next steps would be an integration of a set of full-motion antennas and/or phased array antennas, in the best case starting with adapted customer antennas facilitating a cost-effective global monitoring. What needs further special interest are areas with high consumer traffic as it is reported in the greater London area and/or traffic in areas of merging sea and land traffic in tourist hotspots (concentration of tourist cruise ships interfering with remote area satellite connectivity).

7. CONCLUSION

In this study, we were able to show how the three-dimensional object measurement system algorithms and functionality implemented in the THRIMOS SW can be used to predict, detect and analyse interference between the RF signals of different satellite constellations. The results show that the availability of services via the affected antenna can drop below 99.5% and could become even worse if additional large constellations come into play. As space commercialisation proceeds, this kind of information will become increasingly important for agencies, regulators and satellite operators.

ACKNOWLEDGMENTS

The authors would like to thank the European Space Agency for the co-funding of the THRIMOS development in the ARTES program line and the valuable review discussions of the project work. The authors would also like to thank their project colleagues for their helpful suggestions and review comments regarding the paper.

REFERENCES

[1] *4m LEO Earth Station Antenna*. Calian. URL: https://d26wgh18tyxdzi.cloudfront.net/productResources/4m-LEO-Earth-Station-Antenna.pdf.

[2] Aida, Saika and Kirschner, Michael. “Accuracy Assessment of SGP4 Orbit Information Conversion into Osculating Elements”. In: AIAA/AAS Astrodynamics Specialist Conference and Exhibit. Apr. 2013.

[3] Akhtaruzzaman, Md et al. “Link Budget Analysis in Designing a Web-application Tool for Military X-Band Satellite Communication”. In: *MIST INTERNATIONAL JOURNAL OF SCIENCE AND TECHNOLOGY* 8 (July 2020), pp. 17–33. DOI: 10.47981/j.mijst.08(01)2020.174(17-33).

[4] Cakaj, Shkelzen et al. “The Range and Horizon Plane Simulation for Ground Stations of Low Earth Orbiting (LEO) Satellites”. In: *IJCNS* 4 (Jan. 2011), pp. 585–589. DOI: 10.4236/ijcns.2011.49070.

[5] European Space Agency. *Space Environment Report*. Tech. rep. ESA/ESOC, 2024.

[6] Flohrer, Tim et al. “*Improving ESA’s Collision Risk Estimates by an Assessment of the TLE orbit Errors of the US SSN Catalogue*”. In: Proceedings of the 5th European Conference on Space Debris–5th European Conference on Space Debris, Darmstadt, Germany. Jan. 2009.

[7] *Installation Manual for Sea Tel 5012-91 Ku-Band Broadband-At-Sea VSAT Antenna System*. Page 4. Sea Tel. Nov. 2013.

[8] NASA. *Recommendation for Space Data System Standards; Orbit Data Messages*. Tech. rep. Accessed: 2025-03-19. NASA, 2017. URL: https://www.nasa.gov/wp-content/uploads/2017/12/orbit_data_messages.pdf.

[9] *Satellite direction nameings*. URL: https://blogs.esa.int/orion/2015/01/29/shining-light-on-atv/ (visited on 03/19/2025).

[10] Smith, Malcolm. “Time to turn off the lights”. In: *Nature* 457 (Feb. 2009), p. 27. DOI: 10.1038/457027a.

[11] *Spectrum Analyser SPECTRAN® V6 PLUS 250XA-6*. URL: https://aaronia.com/en/spectran-v6-rsa-250x (visited on 03/19/2025).

[12] Tedeschi, Pietro, Sciancalepore, Savio, and Pietro, Roberto. “Satellite-based communications security: A survey of threats, solutions, and research challenges”. In: *Computer Networks* 216 (Aug. 2022), p. 109246. DOI: 10.1016/j.comnet.2022.109246.

[13] *THE ISO HANDBOOK*. Page 4. ESA. Nov. 2003.

[14] *The LEGION 400 Antenna*. Rev. D. Safran. URL: https://www.analog.com/media/en/technical-documentation/data-sheets/3600fd.pd.

[15] Vallado, David and Crawford, Paul. “SGP4 Orbit Determination”. In: AIAA/AAS Astrodynamics Specialist Conference and Exhibit. Aug. 2008. ISBN: 978-1-62410-001-7. DOI: 10.2514/6.2008-6770.

APPENDIX

Table 3. The availability in % based on the horizon elevation and the duration of the interference. Values below 99.5% are marked in red, values above in green.

Horizon Elevation [°]	50	52	54	56	58	60	62	64	66	68	70	72	74	76	78	80	88.807
Duration [s]																	
2	99.56	99.62	99.67	99.72	99.76	99.79	99.82	99.85	99.88	99.90	99.92	99.93	99.95	99.96	99.98	99.98	99.999785
2.2	99.52	99.58	99.64	99.69	99.73	99.77	99.81	99.84	99.86	99.89	99.91	99.93	99.94	99.96	99.98	99.98	99.999763
2.4	99.48	99.55	99.61	99.66	99.71	99.75	99.79	99.82	99.85	99.88	99.90	99.92	99.94	99.95	99.97	99.98	99.999742
2.6	99.43	99.51	99.57	99.63	99.68	99.73	99.77	99.81	99.84	99.87	99.89	99.91	99.93	99.95	99.97	99.98	99.999720
2.8	99.39	99.47	99.54	99.60	99.66	99.71	99.75	99.79	99.83	99.86	99.88	99.91	99.93	99.95	99.97	99.98	99.999699
3	99.34	99.43	99.51	99.58	99.64	99.69	99.74	99.78	99.82	99.85	99.88	99.90	99.92	99.94	99.97	99.98	99.999677
3.2	99.30	99.39	99.48	99.55	99.61	99.67	99.72	99.76	99.80	99.84	99.87	99.90	99.92	99.94	99.96	99.98	99.999655
3.4	99.26	99.36	99.44	99.52	99.59	99.65	99.70	99.75	99.79	99.83	99.86	99.89	99.91	99.93	99.96	99.97	99.999634
3.6	99.21	99.32	99.41	99.49	99.56	99.63	99.68	99.73	99.78	99.82	99.85	99.88	99.91	99.93	99.96	99.97	99.999612
3.8	99.17	99.28	99.38	99.46	99.54	99.61	99.67	99.72	99.77	99.81	99.84	99.88	99.90	99.93	99.96	99.97	99.999591
4	99.13	99.24	99.34	99.44	99.52	99.59	99.65	99.70	99.75	99.80	99.84	99.87	99.90	99.92	99.96	99.97	99.999569
4.2	99.08	99.20	99.31	99.41	99.49	99.57	99.63	99.69	99.74	99.79	99.83	99.86	99.89	99.92	99.95	99.97	99.999548
4.4	99.04	99.17	99.28	99.38	99.47	99.54	99.61	99.68	99.73	99.78	99.82	99.86	99.89	99.92	99.95	99.97	99.999526
4.6	98.99	99.13	99.25	99.35	99.44	99.52	99.60	99.66	99.72	99.77	99.81	99.85	99.88	99.91	99.95	99.96	99.999505
4.8	98.95	99.09	99.21	99.32	99.42	99.50	99.58	99.65	99.70	99.76	99.80	99.84	99.88	99.91	99.95	99.96	99.999483
5	98.91	99.05	99.18	99.29	99.39	99.48	99.56	99.63	99.69	99.75	99.79	99.84	99.87	99.90	99.94	99.96	99.999462
5.2	98.86	99.01	99.15	99.27	99.37	99.46	99.54	99.62	99.68	99.74	99.79	99.83	99.87	99.90	99.94	99.96	99.999440
5.4	98.82	98.98	99.12	99.24	99.35	99.44	99.53	99.60	99.67	99.73	99.78	99.82	99.86	99.90	99.94	99.96	99.999419
5.6	98.78	98.94	99.08	99.21	99.32	99.42	99.51	99.59	99.66	99.72	99.77	99.82	99.86	99.89	99.94	99.96	99.999397
5.8	98.73	98.90	99.05	99.18	99.30	99.40	99.49	99.57	99.64	99.71	99.76	99.81	99.85	99.89	99.93	99.96	99.999376
6	98.69	98.86	99.02	99.15	99.27	99.38	99.47	99.56	99.63	99.70	99.75	99.80	99.85	99.88	99.93	99.95	99.999354
6.2	98.65	98.83	98.98	99.12	99.25	99.36	99.46	99.54	99.62	99.69	99.75	99.80	99.84	99.88	99.93	99.95	99.999332
6.4	98.60	98.79	98.95	99.10	99.22	99.34	99.44	99.53	99.61	99.68	99.74	99.79	99.84	99.88	99.93	99.95	99.999311
6.6	98.56	98.75	98.92	99.07	99.20	99.32	99.42	99.51	99.59	99.67	99.73	99.78	99.83	99.87	99.93	99.95	99.999289
6.8	98.51	98.71	98.89	99.04	99.18	99.30	99.40	99.50	99.58	99.66	99.72	99.78	99.83	99.87	99.92	99.95	99.999268
7	98.47	98.67	98.85	99.01	99.15	99.28	99.39	99.48	99.57	99.65	99.71	99.77	99.82	99.86	99.92	99.95	99.999246
7.2	98.43	98.64	98.82	98.98	99.13	99.26	99.37	99.47	99.56	99.64	99.70	99.76	99.82	99.86	99.92	99.94	99.999225
7.4	98.38	98.60	98.79	98.96	99.10	99.23	99.35	99.45	99.54	99.63	99.70	99.76	99.81	99.86	99.92	99.94	99.999203
7.6	98.34	98.56	98.76	98.93	99.08	99.21	99.33	99.44	99.53	99.62	99.69	99.75	99.81	99.85	99.91	99.94	99.999182
7.8	98.30	98.52	98.72	98.90	99.05	99.19	99.32	99.42	99.52	99.60	99.68	99.74	99.80	99.85	99.91	99.94	99.999160
8.0	98.25	98.48	98.69	98.87	99.03	99.17	99.30	99.41	99.51	99.59	99.67	99.74	99.80	99.85	99.91	99.94	99.999139
8.2	98.21	98.45	98.66	98.84	99.01	99.15	99.28	99.39	99.50	99.58	99.66	99.73	99.79	99.84	99.91	99.94	99.999117
8.4	98.16	98.41	98.62	98.81	98.98	99.13	99.26	99.38	99.48	99.57	99.65	99.72	99.79	99.84	99.91	99.94	99.999096
8.6	98.12	98.37	98.59	98.79	98.96	99.11	99.25	99.37	99.47	99.56	99.65	99.72	99.78	99.83	99.90	99.93	99.999074
8.8	98.08	98.33	98.56	98.76	98.93	99.09	99.23	99.35	99.46	99.55	99.64	99.71	99.78	99.83	99.90	99.93	99.999053
9	98.03	98.30	98.53	98.73	98.91	99.07	99.21	99.34	99.45	99.54	99.63	99.71	99.77	99.83	99.90	99.93	99.999031
9.2	97.99	98.26	98.49	98.70	98.89	99.05	99.19	99.32	99.43	99.53	99.62	99.70	99.77	99.82	99.90	99.93	99.999009
9.4	97.95	98.22	98.46	98.67	98.86	99.03	99.18	99.31	99.42	99.52	99.61	99.69	99.76	99.82	99.89	99.93	99.998988
9.6	97.90	98.18	98.43	98.64	98.84	99.01	99.16	99.29	99.41	99.51	99.61	99.69	99.76	99.81	99.89	99.93	99.998966
9.8	97.86	98.14	98.39	98.62	98.81	98.99	99.14	99.28	99.40	99.50	99.60	99.68	99.75	99.81	99.89	99.92	99.998945
10	97.81	98.11	98.36	98.59	98.79	98.97	99.12	99.26	99.38	99.49	99.59	99.67	99.74	99.81	99.89	99.92	99.998923